The CARMENES search for exoplanets around M dwarfs. HD147379 b: A nearby Neptune in the temperate zone of an early-M dwarf

Reiners, A.; Ribas, I.; Zechmeister, M.; Caballero, J.A.; Trifonov, T.; Dreizler, S.; ... ; Zapatero Osorio, M.R.

Astronomy & Astrophysics manuscript no. Gl617_corr
December 19, 2017

Letter to the Editor

The CARMENES search for exoplanets around M dwarfs

HD 147379 b: A nearby Neptune in the temperate zone of an early-M dwarf

A. Reiners[1], I. Ribas[2], M. Zechmeister[1], J.A. Caballero[3,4], T. Trifonov[5], S. Dreizler[1], J.C. Morales[2], L. Tal-Or[1], M. Lafarga[2], A. Quirrenbach[4], P.J. Amado[6], A. Kaminski[4], S.V. Jeffers[1], J. Aceituno[7], V.J.S. Béjar[8], J. Guàrdia[2], E.W. Guenther[9], H.-J. Hagen[10], D. Montes[11], V.M. Passegger[1], W. Seifert[4], A. Schweitzer[10], M. Cortés-Contreras[3,11], M. Abril[6], F.J. Alonso-Floriano[11,12], M. Ammler-von Eiff[9,13], R. Antona[6], G. Anglada-Escudé[14], H. Anwand-Heerwart[1], B. Arroyo-Torres[7], M. Azzaro[7], D. Baroch[2], D. Barrado[3], F.F. Bauer[1], S. Becerril[6], D. Benítez[7], Z.M. Berdiñas[6], G. Bergond[7], M. Blümcke[10], M. Brinkmöller[4], C. del Burgo[15], J. Cano[11], M.C. Cárdenas Vázquez[5,6], E. Casal[6], C. Cifuentes[11], A. Claret[6], J. Colomé[2], S. Czesla[10], E. Díez-Alonso[11], C. Feiz[4], M. Fernández[6], I.M. Ferro[6], B. Fuhrmeister[10], D. Galadí-Enríquez[7], A. Garcia-Piquer[2], M.L. García Vargas[16], L. Gesa[2], V. Gómez Galera[7], J.I. González Hernández[8], R. González-Peinado[11], U. Grözinger[5], S. Grohnert[4], A. Guijarro[7], E. de Guindos[7], J. Gutiérrez-Soto[6], A.P. Hatzes[9], P.H. Hauschildt[10], R.P. Hedrosa[7], J. Helmling[7], Th. Henning[5], I. Hermelo[7], R. Hernández Arabí[7], L. Hernández Castaño[7], F. Hernández Hernando[7], E. Herrero[2], A. Huber[5], P. Huke[1], E.N. Johnson[1], E. de Juan[7], M. Kim[4,17], R. Klein[5], J. Klüter[4], A. Klutsch[11,18], M. Kürster[5], F. Labarga[11], A. Lamert[1], M. Lampón[6], L.M. Lara[6], W. Laun[5], U. Lemke[1], R. Lenzen[5], R. Launhardt[5], M. López del Fresno[3], M.J. López-González[6], M. López-Puertas[6], J.F. López Salas[7], J. López-Santiago[19], R. Luque[4], H. Magán Madinabeitia[7], U. Mall[5], L. Mancini[5,20,21], H. Mandel[4], E. Marfil[11], J.A. Marín Molina[7], D. Maroto Fernández[7], E.L. Martín[3], S. Martín-Ruiz[6], C.J. Marvin[1], R.J. Mathar[5], E. Mirabet[6], M.E. Moreno-Raya[7], A. Moya[3], R. Mundt[5], E. Nagel[10], V. Naranjo[5], L. Nortmann[8], G. Nowak[8], A. Ofir[22], R. Oreiro[6], E. Pallé[8], J. Panduro[5], J. Pascual[6], A. Pavlov[5], S. Pedraz[7], A. Pérez-Calpena[16], D. Pérez Medialdea[6], M. Perger[2], M.A.C. Perryman[23], M. Pluto[9], O. Rabaza[6,24], A. Ramón[6], R. Rebolo[8], P. Redondo[8], S. Reffert[4], S. Reinhart[7], P. Rhode[1], H.-W. Rix[5], F. Rodler[5,25], E. Rodríguez[6], C. Rodríguez-López[6], A. Rodríguez Trinidad[6], R.-R. Rohloff[5], A. Rosich[2], S. Sadegi[4], E. Sánchez-Blanco[6], M.A. Sánchez Carrasco[6], A. Sánchez-López[6], J. Sanz-Forcada[3], P. Sarkis[5], L.F. Sarmiento[1], S. Schäfer[1], J.H.M.M. Schmitt[10], J. Schiller[9], P. Schöfer[1], E. Solano[3], O. Stahl[4], J.B.P. Strachan[14], J. Stürmer[4,26], J.C. Suárez[6,24], H.M. Tabernero[11,27], M. Tala[4], S.M. Tulloch[28,29], R.-G. Ulbrich[1], G. Veredas[4], J.I. Vico Linares[7], F. Vilardell[2], K. Wagner[4,5], J. Winkler[9], V. Wolthoff[4], W. Xu[4], F. Yan[5], and M.R. Zapatero Osorio[3]

(Affiliations can be found after the references)

December 19, 2017

ABSTRACT

We report on the first star discovered to host a planet detected by radial velocity (RV) observations obtained within the CARMENES survey for exoplanets around M dwarfs. HD 147379 ($V = 8.9$ mag, $M = 0.58 \pm 0.08\,M_\odot$), a bright M0.0 V star at a distance of 10.7 pc, is found to undergo periodic RV variations with a semi-amplitude of $K = 5.1 \pm 0.4$ m s^{-1} and a period of $P = 86.54 \pm 0.06$ d. The RV signal is found in our CARMENES data, which were taken between 2016 and 2017, and is supported by HIRES/Keck observations that were obtained since 2000. The RV variations are interpreted as resulting from a planet of minimum mass $m_p \sin i = 25 \pm 2\,M_\oplus$, 1.5 times the mass of Neptune, with an orbital semi-major axis $a = 0.32$ au and low eccentricity ($e < 0.13$). HD 147379 b is orbiting inside the temperate zone around the star, where water could exist in liquid form. The RV time-series and various spectroscopic indicators show additional hints of variations at an approximate period of 21.1 d (and its first harmonic), which we attribute to the rotation period of the star.

Key words. Stars: individual: HD 147379 — Planets and satellites: individual: HD 147379 b – Stars: activity – Stars: rotation – Stars: late-type – Stars: low-mass

1. Introduction

Low-mass M-type stars have attracted increasing attention in the exoplanet community over the past decade. The low masses and small radii of M dwarfs make the detection of rocky planets less challenging than for Sun-like stars, and the typical detection limit for radial velocity (RV) surveys is on the order of 1 m s^{-1}, which permits the discovery of rocky planets in their habitable zones (e.g., Martín et al. 2005; Scalo et al. 2007; Tarter et al. 2007; Bonfils et al. 2013; Anglada-Escudé et al. 2016). These stars are also of particular interest because they are by far the most numerous (Henry et al. 2006, 2016). In addition, the transit signal of a rocky planet around such stars is within reach of ground-based telescopes of small aperture (e.g., Gillon et al.

2016; Dittmann et al. 2017), and they are being targeted by upcoming photometry space missions such as *TESS* and *PLATO*.

Until now, RV measurements of M dwarfs have produced 81 planet discoveries in total, many of them in multiple systems.[1] Only 20 of them are more massive than 0.1 $M_{Jupiter}$, suggesting that M dwarfs host fewer giant planets than solar-mass stars (Cumming et al. 2008; Johnson et al. 2010). While this may be a consequence of the hot Jupiters being more frequent around hotter stars because more building material is available (Mordasini et al. 2012), the trend has not been confirmed so far in transit surveys (e.g., Johnson et al. 2012; Obermeier et al. 2016). Low-mass stars are also suspected to favor multi-planet systems, which results in an average of more than two planets per host star (Dressing & Charbonneau 2015). An exoplanet survey targeted on nearby M dwarf stars therefore promises to detect many low-mass planets around nearby stars for which the perspectives for a detailed investigation and characterization are good.

M dwarf stars as targets for exoplanet searches have their specific challenges. While the spectral coverage of typical visual RV instruments is well suited for FGK-type stars, the much redder spectral energy distribution of M-type stars requires red-optical and near-infrared coverage for better efficiency. Additionally, M dwarfs are typically active, and a wide (simultaneous) wavelength coverage is therefore extremely valuable to distinguish between wavelength-dependent activity signals and wavelength-independent planetary signals in RV measurements. CARMENES (Quirrenbach et al. 2014) addresses these issues. We have been conducting a dedicated survey of about 300 well-characterized M dwarfs (Garcia-Piquer et al. 2017; Reiners et al. 2017; Jeffers et al. 2017) since January 2016 within Guaranteed Time Observations. The performance of the instrument has been demonstrated and compared to others in a paper on M-type stars known to host planets (Trifonov et al. 2017). The present paper is dedicated to the first star discovered by CARMENES to host a planet.

In the following, we introduce the host star HD 147379 with its basic properties in Sect. 2, describe our data from CARMENES and HIRES/Keck in Sect. 3, and present our results from the analysis of the radial velocity measurements in combination with various activity indicators in Sect. 4. Our results are then summarized in Sect. 5.

2. HD 147379

The star HD 147379 (GJ 617 A, HIP 79755, J16167+672S) is bright (V = 8.9 mag; J = 5.8 mag) and classified as M0.0 V (Alonso-Floriano et al. 2015); it is located at a distance of d = 10.735 ± 0.026 pc (Gaia Collaboration et al. 2016). This star forms a common proper motion pair with a fainter companion (EW Dra, M3.0 V, V = 10.6 mag) at a projected separation of 1.07 arcmin, or about 690 au at the distance of the system (Lépine & Bongiorno 2007). From the CARMENES data of HD 147379, we detect marginal Doppler broadening caused by rotation with $v \sin i$ = 2.7 ± 1.5 km s^{-1} (Reiners et al. 2017). At this low value of $v \sin i$, we cannot entirely exclude that not rotation, but other effects such as a spectral mismatch between HD 147379 and the reference star caused the additional broadening, which means that the value of $v \sin i$ is essentially an upper limit.

The star shows mild chromospheric Ca H & K emission with a median S-index of 1.53 measured from the HIRES data (Butler et al. 2017). Butler and collaborators reported an absence of Hα emission in most of their spectra, but some Hα emission detections in 12 of their 30 spectra. We cannot confirm this detection in our CARMENES data; all of our spectra show Hα in absorption. We note that Newton et al. (2017) also listed Hα emission for HD 147379, but their reference for this value in fact reported Hα in absorption (Gizis et al. 2002).

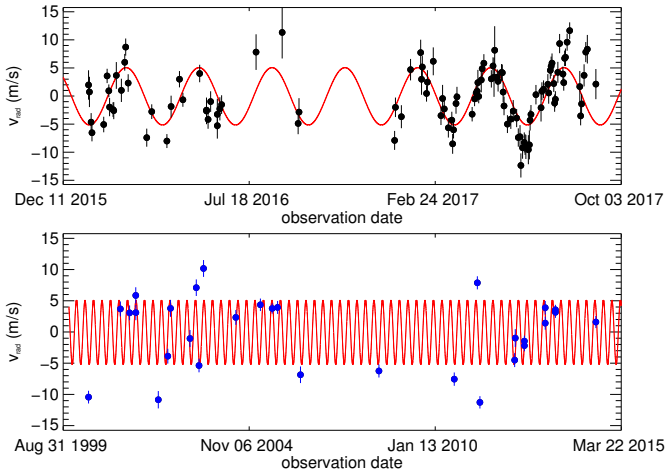

Fig. 1. Radial velocities obtained with CARMENES (upper panel) and HIRES/Keck (lower panel). The orbital motion according to the adopted solution is overplotted in red (see Sect. 4).

Using the ROSAT all-sky survey X-ray flux of GJ 617 A and B (Voges et al. 1999) and the flux ratio derived from a later ROSAT HRI pointing (Schmitt & Liefke 2004), we compute an X-ray luminosity of $L_X = 10^{27.6}$ erg s^{-1} for HD 147379 (GJ 617 A). From the relation between X-ray activity and rotational period given in Eq. 11 in Reiners et al. (2014), we estimate the rotational period to be $P \approx 31$ d. The uncertainty of this estimate is approximately ±20 days because X-ray values of individual stars show a large scatter around the rotation-activity relation.

For the stellar properties, we adopted the values in the top part of Table 1. The atmospheric parameters T_{eff} and [Fe/H] were determined by fitting PHOENIX-ACES synthetic spectra (Husser et al. 2013) to the CARMENES spectra, as described in Passegger et al. (2016). We collected broad-band photometry from several surveys covering all parts of the spectral energy distribution (SED) of the target (Caballero et al. 2016). Integrating this photometric SED allowed us to determine the luminosity L as described in Cifuentes (2017). The radius R was calculated from our measured T_{eff} and L, while the mass was obtained from the linear $M - R$ relation measured by Casal (2014). From the stellar radius and projected equatorial velocity, we can estimate the rotational period of HD 147379 to be $P_{rot}/\sin i = 11^{+15}_{-5}$ d ($f \sin i = 0.09 \pm 0.05$ d^{-1}). If the star is seen under a low inclination angle, i, the real value of P_{rot} will be lower (faster rotation). As explained above, however, the detection of spectral Doppler broadening is only marginal, which means that rotational periods longer than 10–20 d cannot be excluded. A rotation period of 10 d or longer is consistent with the absence of Hα emission; faster rotators ($P_{rot} \leq 10$ d) typically show emission, while slower rotators tend to lose their ability to generate it (Jeffers et al. 2017).

[1] http://exoplanet.eu

3. Data

We analyzed data from the CARMENES VIS channel and HIRES/Keck. The CARMENES measurements were taken in the context of the CARMENES search for exoplanets around M dwarfs. The CARMENES instrument consists of two channels: the VIS channel obtains spectra at a resolution of $R = 94,600$ in the wavelength range 520–960 nm, while the NIR channel yields spectra of $R = 80,400$ covering 960–1710 nm. Both channels are calibrated in wavelength with hollow-cathode lamps and use temperature- and pressure-stabilized Fabry-Pérot etalons to interpolate the wavelength solution and simultaneously monitor the spectrograph drift during nightly operations (Bauer et al. 2015).

Observations with CARMENES were tailored to obtain a signal-to-noise ratio of 150 in the J band, and the typical exposure time for HD 147379 was 7 min. The median internal RV precision of the CARMENES VIS channel exposures of HD 147379 is $\sigma_{\rm VIS} = 1.7\,{\rm m\,s^{-1}}$. The corresponding values of the internal RV precision in the NIR channel are significantly higher, $\sigma_{\rm NIR} = 8.6\,{\rm m\,s^{-1}}$, mainly because in early-M dwarfs the amount of spectral features is higher in the VIS channel spectral range (Reiners et al. 2017). For the analysis carried out in this paper, we therefore only used RVs from the VIS channel. From the CARMENES data, the reduction pipeline provides information about chromospheric emission from Hα, the variation of the line profile shape (dLw), and the chromatic index (crx), as detailed in Zechmeister et al. (2017).

We also computed the cross-correlation function (CCF) of each spectrum using a weighted binary mask that was built from coadded observations of the star itself. We selected ∼3000 deep, narrow, and unblended lines that were weighted according to their contrast and inverse full-width at half-maximum (FWHM). We computed one CCF for each spectral order and subsequently combined these individual CCFs according to the signal-to-noise ratio to compute the final CCF. We fitted a Gaussian function to the central part of the combined CCF and determined the radial velocity, FWHM, contrast, and bisector span. The latter is defined as the difference between the average bisector values in the CCF regions from 90 % to 60 % and from 40 % to 10 %.

We further included in our analysis the RV data from HIRES/Keck published in Butler et al. (2017). Thirty observations are reported between May 2000 and July 2014, and they have a median internal uncertainty of $\sigma_{\rm Keck} = 1.1\,{\rm m\,s^{-1}}$. We show all data in Fig. 1. Butler et al. (2017) reported a signal requiring confirmation at $P = 2.1$ d.

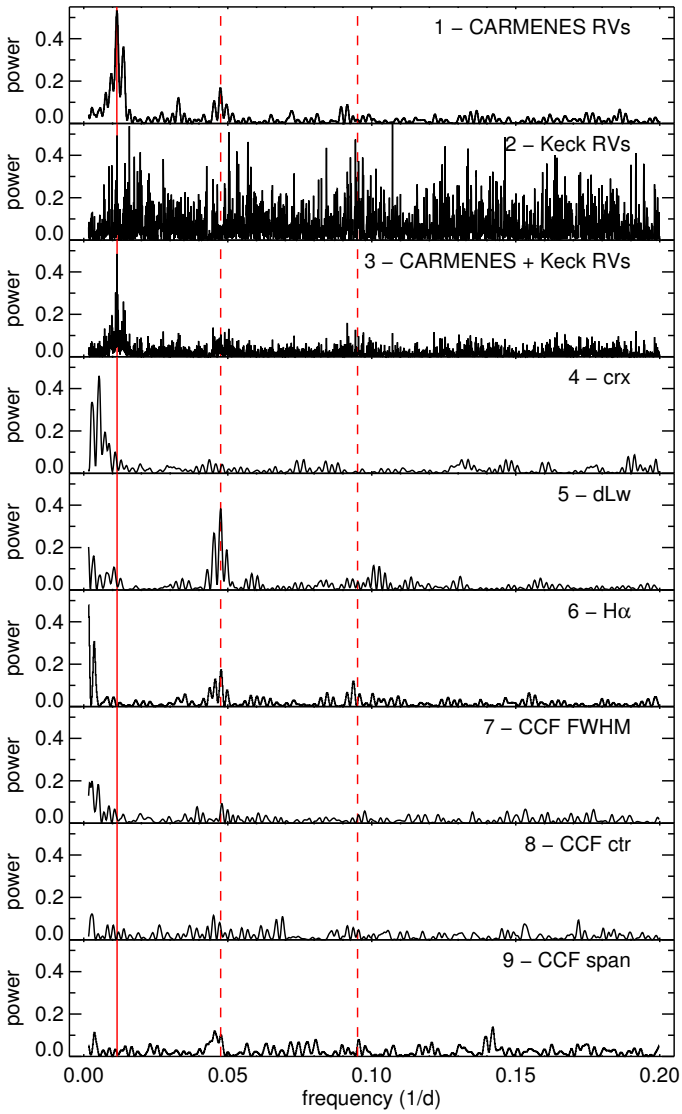

Fig. 2. Periodograms from CARMENES data (top panel), HIRES/Keck data (second panel), and the combined data set (panel 3). The period of 86.5 d is marked with a vertical red line. Panels 4–9 from top to bottom show the chromatic index (crx), the differential line width (dLw), and the Hα index as defined in Zechmeister et al. (2017), and the FWHM, the bisector contrast, and the bisector span from the CCF. Excess power at around $f = 0.047\,{\rm d^{-1}}$ in the CARMENES RVs and dLw is likely caused by stellar rotation (left red dashed line; the right dashed line shows its first harmonic at $f = 0.094\,{\rm d^{-1}}$).

4. Results

We show periodograms using the generalized Lomb-Scargle formalism (GLS, Zechmeister & Kürster 2009) in Fig. 2. In the top panel, CARMENES RVs show a prominent signal at a period of $P = 86.5$ d ($f = 0.0115\,{\rm d^{-1}}$). Because of the limited total time baseline of CARMENES observations, the peak is relatively broad. Keck observations cover a longer time span, which leads to a higher frequency resolution in the periodogram, but the number of observations is not sufficient to identify any statistically significant peak. Nevertheless, we observe excess power at around $f = 0.0115\,{\rm d^{-1}}$, which means that HIRES/Keck data are consistent with a 86.5 d periodicity. The periodogram from both data sets together reveals a clear and unique signal at this frequency, as shown in the third panel of Fig. 2. To test whether the signal is persistent in the CARMENES data, we calculated periodograms from the first and second half of the CARMENES RV data alone. We found the peak at $f = 0.0115\,{\rm d^{-1}}$ in both cases. At $P = 2.1$ d, the period where Butler et al. (2017) reported a signal from their data alone, the CARMENES and combined data sets do not show any signal.

The CARMENES RV periodogram is relatively free of other significant peaks at frequencies longer than $f = 0.02\,{\rm d^{-1}}$ ($P < 50$ d). An interesting group of periodogram peaks appears around $f = 0.047\,{\rm d^{-1}}$ ($P = 21.3$ d). This feature may be connected to the rotational period of the star. We investigated line profile indicators and the Hα index as described in Zechmeister et al. (2017). We note that for the Hα index, we also calculated values when we saw Hα in absorption. Periodograms of the chromatic index (crx), differential line width (dLw), and Hα index are provided in panels 4–6 in Fig. 2, while panels 7–9 show periodograms for the FWHM, the bisector contrast, and the bisector span from

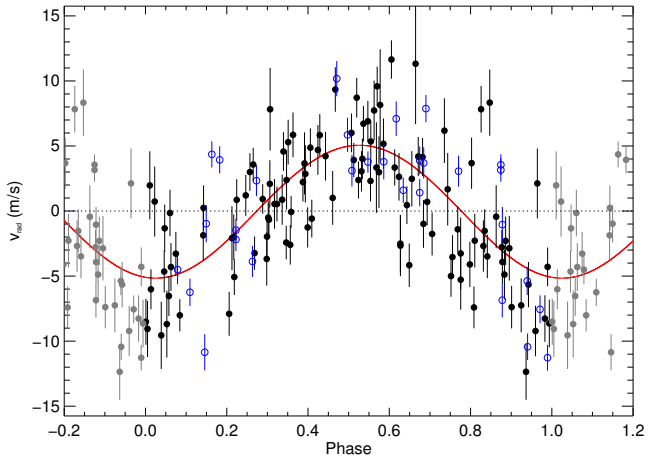

Fig. 3. Phased RVs (black filled circles: CARMENES; blue open circles: HIRES/Keck). The red line shows the orbital motion caused by the planetary companion according to the solution in Table 1. Gray points are repetitions.

the CCF. None of the six indicators show evidence for periodicity at $P = 86.5$ d, but dLw shows signicificant excess power at $P = 21.1$ d. The Hα index and some of the three CCF indices show periodogram peaks around $P = 21.1$ d, $P = 10.6$ d, or both, but no power at $P = 86.5$ d.

From all the gathered evidence, we suspect that the secondary peak at $f = 0.047\,\mathrm{d}^{-1}$ in the CARMENES RVs is caused by rotational modulation of the star that is rotating at $P = 21.1$ d (or $P = 10.6$ d). We note that 21.1 d and 10.6 d are close to the fourth and eighth harmonics of 86.5 d. However, if rotational modulation were the origin of these periodogram peaks, we would also expect the first harmonic around 42 d (and others) to be prominent. Because we do not find this peak, and because we do not find excess power in the activity indicators at $P = 86.5$ d, we conclude that this latter period is of planetary origin.

We determined the parameters of the planet around HD 147379 using a Keplerian model coupled with a Nelder-Mead simplex algorithm (Nelder & Mead 1965; Press et al. 1992), which minimizes the negative logarithm of the model's likelihood function. In our modeling scheme, we also fit for the unknown RV jitter variance σ_{jitter} of the HIRES/Keck and CARMENES data sets, which we incorporated following the recipe in Baluev (2009). We quantified the significance of the signal using the $\Delta \ln L$ statistic, as discussed in Anglada-Escudé et al. (2016). When we used CARMENES data alone, we obtained $\Delta \ln L = 41.7$, which results in a false-alarm probability (FAP) of $\sim 6.2 \times 10^{-15}$. The inclusion of the HIRES/Keck data increased this value to $\Delta \ln L = 51.2$ (FAP of $\sim 1.05 \times 10^{-17}$), meaning that the significance of the detection is further improved by these data. A search for a second signal using the same method did not show evidence for any periodic variability left in the data.

We estimated the uncertainties of the derived orbital parameters by running the Markov chain Monte Carlo (MCMC) sampler `emcee` (Foreman-Mackey et al. 2013) in conjunction with our model, and as the uncertainty, we adopted the 68.3% (1σ) credibility interval of the resulting posterior parameter distribution. The results from our Keplerian modeling of the HD 147379 data are summarized in Table 1, together with the stellar parameters.

Table 1. Parameters of HD 147379 with 1σ uncertainties

Parameter	HD 147479
M ($\mathrm{M}_\odot$)	0.58 ± 0.08
R ($\mathrm{R}_\odot$)	0.57 ± 0.06
L ($\mathrm{L}_\odot$)	0.08 ± 0.01
T_{eff} (K)	4090 ± 50
[Fe/H] (dex)	0.16 ± 0.16
Orbital Solution	
K ($\mathrm{m\,s^{-1}}$)	$5.14^{+0.40}_{-0.48}$
P (d)	$86.54^{+0.07}_{-0.06}$
e	$0.01^{+0.12}_{-0.01}$
ϖ (deg)	93^{+111}_{-122}
M (deg)	59^{+112}_{-123}
t_{trans} (MJD)	$2451665.1^{+4.9}_{-4.1}$
γ_{HIRES} ($\mathrm{m\,s^{-1}}$)	$-1.90^{+0.76}_{-0.80}$
$\gamma_{\mathrm{CARM.}}$ ($\mathrm{m\,s^{-1}}$)	$0.78^{+0.36}_{-0.32}$
$\sigma_{\mathrm{jitter,HIRES}}$ ($\mathrm{m\,s^{-1}}$)	$3.7^{+1.0}_{-0.2}$
$\sigma_{\mathrm{jitter,CARMENES}}$ ($\mathrm{m\,s^{-1}}$)	$2.9^{+0.4}_{-0.17}$
a (au)	$0.3193^{+0.0002}_{-0.0002}$
$m_{\mathrm{P}} \sin i$ ($M_\oplus$)	$24.7^{+1.8}_{-2.4}$

In Fig. 3 we show the phased RVs together with the best fit that includes additional RV jitter. The total jitter, $(\sigma^2_{\mathrm{int}} + \sigma^2_{\mathrm{jitter}})^{1/2}$, is on the order of 3–4 $\mathrm{m\,s^{-1}}$ for both instruments. The jitter term determined for the HIRES data is consistent with the term reported by Isaacson & Fischer (2010) for the HIRES data of HD 147379. We also tried a model fit considering no RV jitter. All resulting parameters are well within the 1σ error bars of those listed in Table 1 except for the eccentricity and the argument of periastron. The model including jitter yields an orbital solution with low eccentricity ($e < 0.13$), while the model with no jitter results in a rather high eccentricity ($e = 0.29$). We favor the model that considers RV jitter under the assumption that there is only one detectable planet orbiting the star and that all the RV noise is a combination of stellar jitter and instrumental noise systematics.

The best-fit orbital solution yields a planetary companion of mass $m_{\mathrm{P}} \sin i \approx 25\,\mathrm{M}_\oplus$ with an orbital semi-major axis $a = 0.32$ au and low eccentricity, which locates the planet inside the liquid-water temperate zone around HD 147379 (Kopparapu et al. 2013, 2014). According to our MCMC posterior distribution, however, the planetary eccentricity is poorly constrained, and within 2σ, we find that $e < 0.25$. We note that such a high eccentricity for HD 147379 b would cause the planet to approach the star at closer than the habitable-zone limit near the periastron orbital phase. The best-fit orbit of HD 147379 b is depicted in Fig. 4 together with the limits of the conservative habitable zone.[2]

After subtracting the orbital motion caused by HD 147379 b from the observed RVs, we calculated the residual periodogram for the CARMENES, HIRES/Keck, and combined data sets (Fig. B.1). The resulting periodograms show no significant additional periodicities. Our analysis indicates that any possible

[2] http://depts.washington.edu/naivpl/sites/default/files/hz.shtml

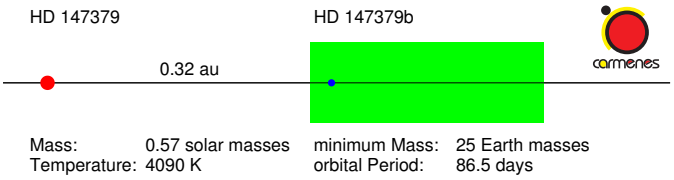

Fig. 4. Visualization of HD 147379 (red circle) and its planet (blue circle). The green area indicates the conservative habitable-zone limits.

further planet in the system should have an RV amplitude significantly below $\sim$2 m s^{-1}.

5. Conclusions

Radial velocity observations of HD 147379 reveal a 25-$M_\oplus$ planet in the temperate zone around this early-M star. HD 147379 is the first star discovered to host a planet by the CARMENES search for exoplanets around M dwarfs. The existence of the planet and its orbital parameters are supported by RV observations from HIRES/Keck.

With a mass between those of Saturn and Neptune ($m_{\rm HD\,147379\,b} \approx 0.3\,M_{\rm Saturn} \approx 1.5\,M_{\rm Neptune}$), HD 147379 b occupies a mass range that is relatively poorly populated, especially around stars that are significantly less massive than the Sun. This planet is located in mass between the super-Earths that grow large enough to open a gap in the disk for type II migration but cannot continue accreting, and the "main clump" planets that can trigger runaway gas accretion and rapidly grow larger (Mordasini et al. 2009). HD 147379 b is similar to the known planets GJ 436 b (Butler et al. 2004), GJ 3293 b (Astudillo-Defru et al. 2015), GJ 229 b, and GJ 433 c (Tuomi et al. 2014), but is located inside the temperate zone of its host star.

The astrometric motion of HD 147379 is relatively large, and the star is a good candidate for determining orbital motion with *Gaia* in a low-mass star. When we assume that the orbit is circular, the lower limit for the orbital motion semi-amplitude of HD 147379 that is caused by HD 147379 b and seen from Earth is 4.1 μas. If the system is seen under inclination angles lower than $i = 90$ deg, the mass of the planet is higher, and so is the astrometric orbit. The expected performance of *Gaia* astrometry for HD 147379 is 6.8 μas.[3] Thus, astrometric detection of the orbital motion of HD 147379 caused by its planet is likely possible with *Gaia*.

HD 147379 b would be extremely valuable in terms of characterization potential if it transits its host star. The expected transit depth is of 5–10 mmag, but it has a low geometric transit probability of only 0.8%. Photometric follow-up from the ground is complicated by the long period and correspondingly extended transit duration and the uncertainty of the conjunction phase. Nevertheless, it lies only 10 deg away from the ecliptic pole, and *TESS* should be able to determine whether transits occur.

The discovery of HD 147379 b demonstrates the advantage of programs designed to find planets in orbits of days to months, which are particularly critical for exploring the habitability zone of M dwarfs. The discovery also shows that some of these planets have likely been missed in previous searches.

Acknowledgements. We thank an anonymous referee for prompt attention and helpful comments. CARMENES is an instrument for the Centro Astronómico Hispano-Alemán de Calar Alto (CAHA, Almería, Spain). CARMENES is funded by the German Max-Planck-Gesellschaft (MPG), the Spanish Consejo Superior de Investigaciones Científicas (CSIC), the European Union through FEDER/ERF FICTS-2011-02 funds, and the members of the CARMENES Consortium (Max-Planck-Institut für Astronomie, Instituto de Astrofísica de Andalucía, Landessternwarte Königstuhl, Institut de Ciències de l'Espai, Insitut für Astrophysik Göttingen, Universidad Complutense de Madrid, Thüringer Landessternwarte Tautenburg, Instituto de Astrofísica de Canarias, Hamburger Sternwarte, Centro de Astrobiología and Centro Astronómico Hispano-Alemán), with additional contributions by the Spanish Ministry of Economy, the German Science Foundation through the Major Research Instrumentation Programme and DFG Research Unit FOR2544 "Blue Planets around Red Stars", the Klaus Tschira Stiftung, the states of Baden-Württemberg and Niedersachsen, and by the Junta de Andalucía. We acknowledge the following funding programs: European Research Council (ERC-279347), Deutsche Forschungsgemeinschaft (RE 1664/12-1, RE 2694/4-1), Bundesministerium für Bildung und Forschung (BMBF-05A14MG3, BMBF-05A17MG3), Spanish Ministry of Economy and Competitiveness (MINECO, grants AYA2015-68012-C2-2-P, AYA2016-79425-C3-1,2,3-P, AYA2015-69350-C3-2-P, AYA2014-54348-C03-01, AYA2014-56359-P, AYA2014-54348-C3-2-R, AYA2016-79425-C3-3-P and 2013 Ramòn y Cajal program RYC-2013-14875), Fondo Europeo de Desarrollo Regional (FEDER, grant ESP2016-80435-C2-1-R, ESP2015-65712- C5-5-R), Generalitat de Catalunya/CERCA programme, Spanish Ministerio de Educación, Cultura y Deporte, programa de Formación de Profesorado Universitario (grant FPU15/01476), Deutsches Zentrum für Luft- und Raumfahrt (grants 50OW0204 and 50OO1501), Office of Naval Research Global (award no. N62909-15-1-2011), Mexican CONACyT grant CB-2012-183007.

[3] https://www.cosmos.esa.int/web/gaia/science-performance

References

Alonso-Floriano, F. J., Morales, J. C., Caballero, J. A., et al. 2015, A&A, 577, A128
Anglada-Escudé, G., Amado, P. J., Barnes, J., et al. 2016, Nature, 536, 437
Astudillo-Defru, N., Bonfils, X., Delfosse, X., et al. 2015, A&A, 575, A119
Baluev, R. V. 2009, MNRAS, 393, 969
Bauer, F. F., Zechmeister, M., & Reiners, A. 2015, A&A, 581, A117
Bonfils, X., Delfosse, X., Udry, S., et al. 2013, A&A, 549, A109
Butler, R. P., Vogt, S. S., Laughlin, G., et al. 2017, AJ, 153, 208
Butler, R. P., Vogt, S. S., Marcy, G. W., et al. 2004, ApJ, 617, 580
Caballero, J. A., Cortés-Contreras, M., Alonso-Floriano, F. J., et al. 2016, in 19th Cambridge Workshop on Cool Stars, Stellar Systems, and the Sun (CS19), 148
Casal, E. 2014, Master's thesis, Universidad de La Laguna, Spain
Cifuentes, C. 2017, Master's thesis, Universidad Compultense Madrid, Spain
Cumming, A., Butler, R. P., Marcy, G. W., et al. 2008, PASP, 120, 531
Dittmann, J. A., Irwin, J. M., Charbonneau, D., et al. 2017, Nature, 544, 333
Dressing, C. D. & Charbonneau, D. 2015, ApJ, 807, 45
Foreman-Mackey, D., Hogg, D. W., Lang, D., & Goodman, J. 2013, PASP, 125, 306
Gaia Collaboration, Brown, A. G. A., Vallenari, A., et al. 2016, A&A, 595, A2
Garcia-Piquer, A., Morales, J. C., Ribas, I., et al. 2017, A&A, 604, A87
Gillon, M., Jehin, E., Lederer, S. M., et al. 2016, Nature, 533, 221
Gizis, J. E., Reid, I. N., & Hawley, S. L. 2002, AJ, 123, 3356
Henry, T. J., Jao, W.-C., Subasavage, J. P., et al. 2006, AJ, 132, 2360
Henry, T. J., Jao, W.-C., Winters, J. G., et al. 2016, in American Astronomical Society Meeting Abstracts, Vol. 227, American Astronomical Society Meeting Abstracts, 142.01
Husser, T.-O., Wende-von Berg, S., Dreizler, S., et al. 2013, A&A, 553, A6
Isaacson, H. & Fischer, D. 2010, ApJ, 725, 875
Jeffers, S. V., Schöfer, P., Lamert, A., et al. 2017, A&A, submitted
Johnson, J. A., Aller, K. M., Howard, A. W., & Crepp, J. R. 2010, PASP, 122, 905
Johnson, J. A., Gazak, J. Z., Apps, K., et al. 2012, AJ, 143, 111
Kopparapu, R. K., Ramirez, R., Kasting, J. F., et al. 2013, ApJ, 765, 131
Kopparapu, R. K., Ramirez, R. M., SchottelKotte, J., et al. 2014, ApJ, 787, L29
Lépine, S. & Bongiorno, B. 2007, AJ, 133, 889
Martín, E. L., Guenther, E., Barrado y Navascués, D., et al. 2005, Astronomische Nachrichten, 326, 1015
Mordasini, C., Alibert, Y., & Benz, W. 2009, A&A, 501, 1139
Mordasini, C., Alibert, Y., Benz, W., Klahr, H., & Henning, T. 2012, A&A, 541, A97
Nelder, J. A. & Mead, R. 1965, Computer Journal, 7, 308
Newton, E. R., Irwin, J., Charbonneau, D., et al. 2017, ApJ, 834, 85
Obermeier, C., Koppenhoefer, J., Saglia, R. P., et al. 2016, A&A, 587, A49
Passegger, V. M., Wende-von Berg, S., & Reiners, A. 2016, A&A, 587, A19
Press, W. H., Teukolsky, S. A., Vetterling, W. T., & Flannery, B. P. 1992, Numerical recipes in FORTRAN. The art of scientific computing

Quirrenbach, A., Amado, P. J., Caballero, J. A., et al. 2014, in Proc. SPIE, Vol. 9147, Ground-based and Airborne Instrumentation for Astronomy V, 91471F

Reiners, A., Schüssler, M., & Passegger, V. M. 2014, ApJ, 794, 144

Reiners, A., Zechmeister, M., Caballero, J. A., et al. 2017, ArXiv e-prints [arXiv:1711.06576]

Scalo, J., Kaltenegger, L., Segura, A. G., et al. 2007, Astrobiology, 7, 85

Schmitt, J. H. M. M. & Liefke, C. 2004, A&A, 417, 651

Tarter, J. C., Backus, P. R., Mancinelli, R. L., et al. 2007, Astrobiology, 7, 30

Trifonov, T., Kürster, M., Zechmeister, M., et al. 2017, ArXiv e-prints [arXiv:1710.01595]

Tuomi, M., Jones, H. R. A., Barnes, J. R., Anglada-Escudé, G., & Jenkins, J. S. 2014, MNRAS, 441, 1545

Voges, W., Aschenbach, B., Boller, T., et al. 1999, A&A, 349, 389

Zechmeister, M. & Kürster, M. 2009, A&A, 496, 577

Zechmeister, M., Reiners, A., Amado, P. J., et al. 2017, A&A, accepted

[1] Institut für Astrophysik, Georg-August-Universität, Friedrich-Hund-Platz 1, D-37077 Göttingen, Germany
e-mail: Ansgar.Reiners@phys.uni-goettingen.de
[2] Institut de Ciències de l'Espai (CSIC-IEEC), Campus UAB, c/ de Can Magrans s/n, E-08193 Bellaterra, Barcelona, Spain
[3] Centro de Astrobiología (CSIC-INTA), Instituto Nacional de Técnica Aeroespacial, Ctra. de Torrejón a Ajalvir, km 4, E-28850 Torrejón de Ardoz, Madrid, Spain
[4] Zentrum für Astronomie der Universtät Heidelberg, Landessternwarte, Königstuhl 12, D-69117 Heidelberg, Germany
[5] Max-Planck-Institut für Astronomie, Königstuhl 17, D-69117 Heidelberg, Germany
[6] Instituto de Astrofísica de Andalucía (IAA-CSIC), Glorieta de la Astronomía s/n, E-18008 Granada, Spain
[7] Centro Astronómico Hispano-Alemán (CSIC-MPG), Observatorio Astronómico de Calar Alto, Sierra de los Filabres, E-04550 Gérgal, Almería, Spain
[8] Instituto de Astrofísica de Canarias, Vía Láctea s/n, 38205 La Laguna, Tenerife, Spain, and Departamento de Astrofísica, Universidad de La Laguna, E-38206 La Laguna, Tenerife, Spain
[9] Thüringer Landessternwarte Tautenburg, Sternwarte 5, D-07778 Tautenburg, Germany
[10] Hamburger Sternwarte, Gojenbergsweg 112, D-21029 Hamburg, Germany
[11] Departamento de Astrofísica y Ciencias de la Atmósfera, Facultad de Ciencias Físicas, Universidad Complutense de Madrid, E-28040 Madrid, Spain
[12] Leiden Observatory, Leiden University, Postbus 9513, 2300 RA, Leiden, The Netherlands
[13] Max-Planck-Institut für Sonnensystemforschung, Justus-von-Liebig-Weg 3, D-37077 Göttingen, Germany
[14] School of Physics and Astronomy, Queen Mary, University of London, 327 Mile End Road, London, E1 4NS
[15] Instituto Nacional de Astrofísica, Óptica y Electrónica, Luis Enrique Erro 1, Sta. Ma. Tonantzintla, Puebla, Mexico
[16] FRACTAL SLNE. C/ Tulipán 2, P13-1A, E-28231 Las Rozas de Madrid, Spain
[17] Institut für Theoretische Physik und Astrophysik, Leibnizstraße 15, D-24118 Kiel, Germany
[18] Osservatorio Astrofisico di Catania, Via S. Sofia 78, 95123 Catania, Italy
[19] Dpto. de Teoría de la Señal y Comunicaciones, Universidad Carlos III de Madrid, Escuela Politécnica Superior, Avda. de la Universidad, 30. E-28911 Leganés, Madrid, Spain
[20] Dipartimento di Fisica, Unversità di Roma, "Tor Vergata", Via della Ricerca Scientifica, 1 - 00133 Roma, Italy
[21] INAF, Osservatorio Astrofisico di Torino, via Osservatorio 20, 10025, Pino Torinese, Italy
[22] Weizmann Institute of Science, 234 Herzl Street, Rehovot 761001, Israel
[23] University College Dublin, School of Physics, Belfield, Dublin 4, Ireland
[24] Universidad de Granada, Av. del Hospicio, s/n, E-18010 Granada, Spain
[25] European Southern Observatory, Alonso de Córdova 3107, Vitacura, Casilla 19001, Santiago de Chile, Chile
[26] The University of Chicago, Edward H. Levi Hall, 5801 South Ellis Avenue, Chicago, Illinois 60637, USA
[27] Dpto. de Física, Ingeniería de Sistemas y Teoría de la Señal, Escuela Politécnica Superior, Universidad de Alicante, Apdo.99, E-03080, Alicante, Spain
[28] QUCAM Astronomical Detectors, http://www.qucam.com/
[29] European Southern Observatory, Karl-Schwarzschild-Str. 2, D-85748 Garching bei München

Appendix A: CARMENES radial velocities

Appendix B: Residuals

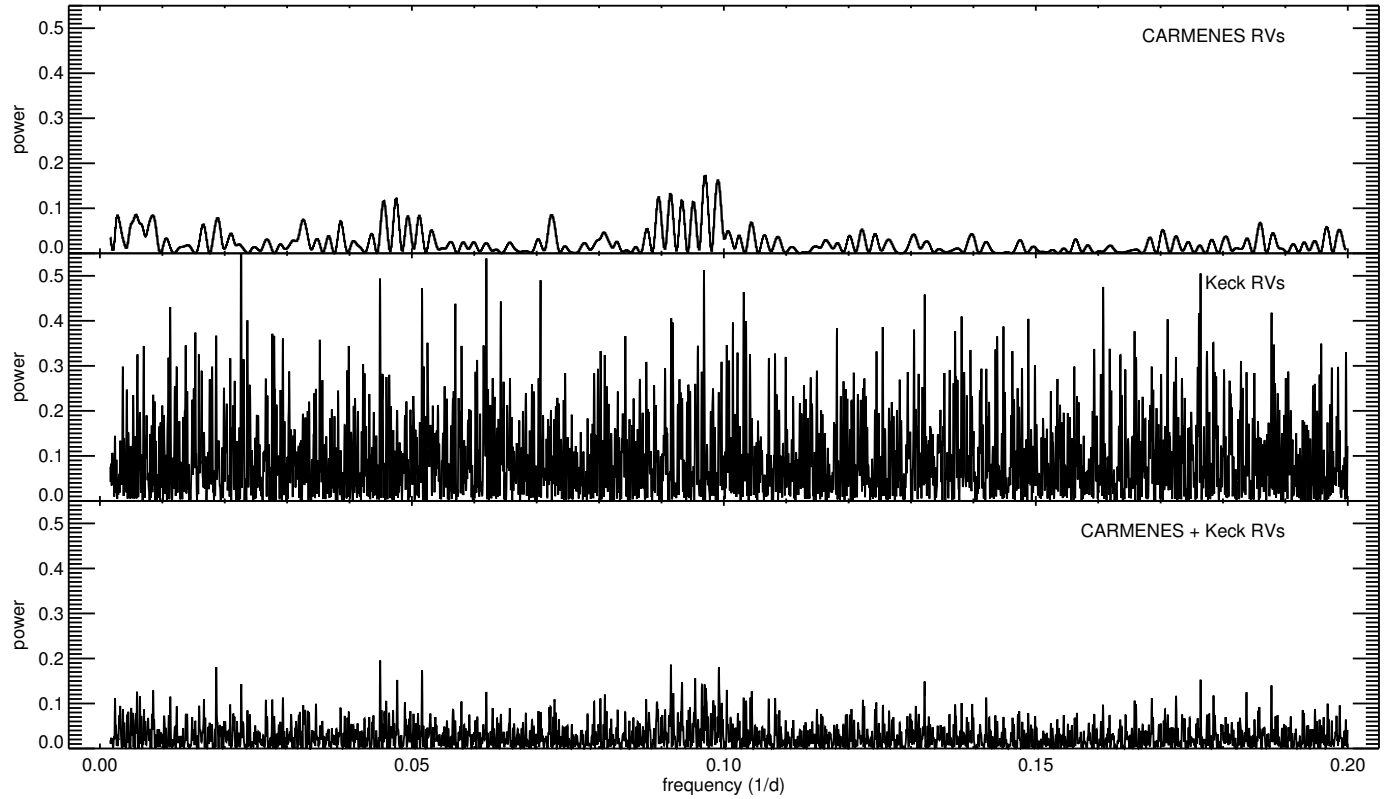

Fig. B.1. Periodogram of residuals after removing the 86.5 d planet signal.

Table A.1. Modified Julian Date and CARMENES radial velocities for HD 147379

MJD	$v_{\rm rad}$ (m/s)
2457397.691	1.97 ± 2.62
2457398.734	0.73 ± 2.69
2457400.753	−4.65 ± 1.61
2457401.754	−6.53 ± 1.53
2457415.688	−5.07 ± 1.38
2457419.712	3.58 ± 1.28
2457421.735	0.93 ± 1.14
2457422.656	−1.97 ± 1.62
2457426.748	−2.42 ± 1.30
2457427.606	−2.60 ± 1.52
2457430.636	3.66 ± 2.39
2457436.638	1.01 ± 2.07
2457440.635	6.01 ± 1.49
2457441.761	8.71 ± 1.53
2457444.691	2.31 ± 1.57
2457466.729	−7.41 ± 1.61
2457472.672	−2.78 ± 1.31
2457490.622	−8.01 ± 1.24
2457495.612	−1.86 ± 1.93
2457505.552	3.00 ± 1.45
2457509.598	−0.66 ± 1.26
2457529.506	4.01 ± 1.56
2457537.597	−2.50 ± 2.21
2457537.609	−2.66 ± 2.35
2457539.486	−4.16 ± 1.67
2457542.512	−0.99 ± 1.84
2457550.436	−3.26 ± 2.77
2457550.446	−5.28 ± 2.30
2457553.441	−2.28 ± 2.06
2457555.545	−1.53 ± 1.67
2457596.397	7.82 ± 3.17
2457627.374	11.32 ± 4.64
2457646.299	−4.88 ± 1.91
2457647.334	−2.86 ± 2.48
2457760.750	−7.90 ± 1.69
2457761.734	−2.01 ± 1.74
2457768.751	−3.68 ± 2.05
2457779.650	4.69 ± 1.91
2457791.624	7.73 ± 2.30
2457792.653	2.99 ± 2.76
2457793.614	5.17 ± 1.95
2457798.605	0.46 ± 1.45
2457799.659	2.48 ± 2.12
2457806.595	6.18 ± 2.48
2457815.733	−3.49 ± 1.68
2457817.621	−0.44 ± 2.42
2457819.635	−2.29 ± 1.87
2457824.500	−5.65 ± 1.74
2457828.575	−4.29 ± 1.49
2457829.561	−8.51 ± 1.77
2457830.634	−6.02 ± 1.54
2457833.562	−1.33 ± 1.82
2457834.691	−0.15 ± 1.79
2457852.703	−3.23 ± 1.28
2457855.608	−0.50 ± 1.30
2457857.475	0.54 ± 1.34
2457858.579	0.87 ± 1.92
2457859.513	2.38 ± 2.27
2457860.486	−0.07 ± 1.23
2457863.518	2.86 ± 2.20
2457864.588	4.87 ± 1.48

Table A.1. continued.

MJD	$v_{\rm rad}$ (m/s)
2457866.595	5.83 ± 1.62
2457875.474	3.05 ± 1.55
2457877.458	5.35 ± 1.54
2457878.651	3.34 ± 3.48
2457879.447	8.15 ± 4.28
2457882.548	3.35 ± 1.39
2457883.466	2.63 ± 1.83
2457887.560	4.19 ± 1.50
2457888.486	4.15 ± 1.47
2457889.462	0.70 ± 1.80
2457890.516	−1.76 ± 1.66
2457894.539	−5.00 ± 1.59
2457898.555	−4.10 ± 1.74
2457901.431	−2.69 ± 1.97
2457905.484	−3.92 ± 1.62
2457907.447	−7.39 ± 1.64
2457909.487	−7.25 ± 2.07
2457910.522	−12.36 ± 2.15
2457912.536	−9.22 ± 1.94
2457914.540	−8.27 ± 1.79
2457915.479	−8.64 ± 1.83
2457916.443	−9.06 ± 2.15
2457919.364	−9.55 ± 2.59
2457920.560	−8.69 ± 2.58
2457921.435	−4.30 ± 1.84
2457922.478	−3.28 ± 1.68
2457928.374	0.24 ± 1.73
2457934.424	−2.08 ± 2.46
2457935.443	0.86 ± 1.59
2457937.365	1.21 ± 1.58
2457942.496	2.09 ± 1.82
2457943.494	0.55 ± 1.91
2457945.397	4.58 ± 1.49
2457946.399	5.30 ± 1.72
2457947.432	5.86 ± 1.72
2457949.540	2.22 ± 1.49
2457950.548	−1.26 ± 1.54
2457951.431	−0.58 ± 1.45
2457954.352	4.22 ± 1.87
2457956.438	9.34 ± 1.71
2457960.373	3.92 ± 1.31
2457961.368	2.38 ± 1.43
2457962.425	6.71 ± 1.37
2457963.373	6.90 ± 1.56
2457965.352	9.58 ± 1.52
2457968.395	11.65 ± 1.47
2457980.374	1.67 ± 2.79
2457981.388	−3.54 ± 1.68
2457982.513	−1.40 ± 1.76
2457985.463	3.68 ± 1.97
2457987.489	7.83 ± 1.79
2457989.331	8.33 ± 2.54
2457999.464	2.12 ± 2.69